ROCK inhibition promotes axon and myelin regeneration via PI3K/Akt/GSK3β in a mouse sciatic nerve injury model

SHUANG DOU[1*], ZHIJUN LI[2*], BOYAO ZHENG[1], ZHENYU REN[3], HAI WANG[3], QING ZUO[1], FANG FANG[2] and YUEHONG ZHUANG[1]

[1]Institute of Clinical Applied Anatomy, Fujian Key Laboratory of Brain Aging and Neurodegenerative Diseases, School of Basic Medical Sciences, Fujian Medical University, Fuzhou, Fujian 350122, P.R. China;
[2]Department of Pharmacology, Fujian Medical University, Fuzhou, Fujian 350122, P.R. China;
[3]Orthopedic Department, First Affiliated Hospital, Fujian Medical University, Fuzhou, Fujian 350108, P.R. China

Received August 28, 2025; Accepted October 16, 2025

DOI: 10.3892/ijmm.2025.5685

Abstract. The present study investigates the molecular mechanisms of peripheral nerve regeneration by examining the ROCK/PI3K/Akt/GSK3β pathway's role in promoting morphological and functional recovery after peripheral nerve injury (PNI). Using a mouse sciatic nerve crush (SNC) injury model and a dorsal root ganglion (DRG) explant axotomy model, mice and DRG were divided the experimental (treated with DMSO) group, Y27632 group (treated with ROCK inhibitor Y27632), Y + LY group (treated with Y27632 + PI3K inhibitor LY294002), and Y + LY + SB group (treated with Y27632 + LY294002 + GSK3β inhibitor SB216763). Immunofluorescence was used to assess axon density, diameter, myelin thickness and Schwann cell proliferation, while retrograde tracing with cholera toxin subunit B evaluated peripheral-to-central reconnection. Behavioral tests measured functional recovery, and in DRG explants, axon regeneration length and growth cone size were quantified. Protein expression analysis of RhoA, ROCK, PI3K, Akt, GSK3β, and their phosphorylated forms was conducted on day 3 post-axotomy, both *in vivo* and *in vitro*. Additionally, RSC96 Schwann cell migration and proliferation were evaluated using scratch assays and EdU staining. Results showed that ROCK inhibition with Y27632 significantly enhanced axonal regeneration, growth cone expansion, retrograde transport, and reinnervation of acetylcholine receptors and Merkel cells, and promoted Schwann cell proliferation and RSC96 migration, leading to thicker myelin sheaths after SNC. These changes mitigated gastrocnemius muscle atrophy, improved muscle strength, gait, and thermal/tactile sensitivity. Co-treatment with LY294002 blocked these effects, but adding SB216763 restored them. Protein analysis indicated that ROCK inhibition increased phosphorylated PI3K, Akt and GSK3β, whereas PI3K inhibition reduced GSK3β phosphorylation. These findings suggested that ROCK inhibition promotes axon regeneration and remyelination after PNI by enhancing PI3K/Akt phosphorylation and suppressing GSK3β activity, highlighting the therapeutic potential of targeting the ROCK/PI3K/Akt/GSK3β pathway for peripheral nerve repair.

Correspondence to: Dr Yuehong Zhuang, Institute of Clinical Applied Anatomy, Fujian Key Laboratory of Brain Aging and Neurodegenerative Diseases, School of Basic Medical Sciences, Fujian Medical University, 1 Xuefu North Road, Minhou University District, Fuzhou, Fujian 350122, P.R. China
E-mail: zhuanghyuehong@163.com

*Contributed equally

Key words: peripheral nerve injury, ROCK/PI3K/Akt/GSK3β, axon regeneration, remyelination, growth cone

Introduction

Peripheral nerve injury (PNI) is a major cause of long-term disability worldwide, with an annual incidence estimated between 1.46-2.8% (1), and accounting for 2.8% of traumatic injuries (2). PNI can impose substantial physical and socioeconomic burdens in several ways. Firstly, it triggers rapid skeletal muscle atrophy, with the cross-sectional area (CSA) of skeletal muscles reduced by up to 75% within months (3). Secondly, prevalent sensory dysfunction is evident, as 50% of patients experience neuropathic pain after traumatic injury in the upper extremities. Thirdly, it incurs a considerable financial burden, as indicated by an average sick-leave duration of 147 days and socioeconomic costs amounting to 197€ per day (4).

In the past decades, significant progress has been made in microsurgical techniques for repairing injured nerves, which, in some cases, has led to improved outcomes (5). However, functional recovery often remains suboptimal following PNI. After such nerve injuries, the injured neurons must regenerate their axons over long distances at an extremely slow rate of ~1 mm per day (6). At this sluggish pace, re-establishing functional motor units or reinnervating sensory organs can take several months or even years, a condition termed chronic axotomy, which frequently results in poor prognosis (7). Therefore, identifying strategies to accelerate axon regeneration and enhance therapeutic outcomes is of considerable significance.

RhoA, a small GTPase, becomes activated upon binding to GTP, thereby activating the downstream Rho kinase (also known as Rho-associated coiled-coil containing protein kinase, ROCK), a serine/threonine protein kinase existing in two subtypes: ROCK1 and ROCK2 (8). The RhoA/ROCK pathway regulates actin and microtubule dynamics by phosphorylating the myosin light chain (MLC) and LIM kinase (9). During axon growth, inhibition of the RhoA/ROCK pathway reduces actin contraction, thereby promoting axon growth and regeneration (10). Additionally, this pathway influences axonal growth through crosstalk with other signaling pathways, most notably by inhibiting the PI3K/Akt pathway to impede axon outgrowth. One investigation demonstrated that ROCK inhibition could reduce flap necrosis and promote cutaneous nerve regeneration by activating the PI3K/Akt pathway (11). Another study showed that ROCK inhibition could significantly enhance axonal regeneration and remyelination, as well as motor and sensory functional recovery in a rat sciatic nerve (SN) transection model by activating the PI3K/Akt pathway (12). However, the downstream targets of the ROCK/PI3K/Akt pathway involved in regulating axon regeneration remain undefined.

Numerous studies indicate that well-characterized downstream molecules of the PI3K/Akt pathway regulating axonal growth include GSK-3β (13), mTOR (14) and FoxO3a (15). Among these, GSK-3β directly participates in the regulation of cytoskeletal microtubule dynamics (13). Activation of the PI3K/Akt pathway phosphorylates GSK-3β at serine residues 9 (16), reducing its kinase activity, resulting in alleviated inhibition on microtubule-associated proteins, such as CRMP-2, MAP1B and APC (17-19), thereby stabilizing growth cone microtubules and promoting axonal extension. In the present study, it was aimed to investigate whether GSK-3β acts as a downstream mediator of the PI3K/Akt pathway, contributing to the effects of ROCK inhibition on axonal regeneration, myelin repair, and functional recovery following SN injury.

Materials and methods

Animal model and experimental groups. All animal procedures were approved by the Experimental Animal Ethics Committee of Fujian Medical University (approval no. 2024-Y-0566; Fuzhou, CHina) and complied with the National Institutes of Health guidelines and ARRIVE standards. 96 male ICR mice (22±3 g, 6 weeks old) were used and housed under standard conditions with *ad libitum* access to food and water. After anesthesia with sodium pentobarbital [50 mg/kg, intraperitoneal injection (i.p.)], a SN crush (SNC) injury model was established by exposing the right SN at the level of the biceps femoris tendon and applying constant pressure for 1 min using hemostatic forceps. Mice were randomized into four groups: i) Experimental group (DMSO, i.p.); ii) Y27632 group (ROCK inhibitor Y27632); iii) Y + LY group (Y27632 + PI3K inhibitor LY294002); and iv) Y + LY + SB group (Y27632 + LY294002 + GSK3β inhibitor SB216763). All compounds were purchased from Shanghai Aladdin Biochemical Technology Co., Ltd. and administered i.p. at a dose of 10 mg/kg. Additionally, a Sham group in which the SN was exposed but not crushed was included. Mice were sacrificed with an overdose of sodium pentobarbital (≥150 mg/kg, i.p.) at specified time points (days 1, 3, 5, 14, and 30), with six animals per group per time point for histological or biochemical analyses. Death was confirmed by the cessation of heartbeat and respiration, as well as absence of corneal and pedal reflexes.

Dorsal root ganglion (DRG) explant culture and axotomy. Dorsal root ganglia (DRG) were isolated from E15 Sprague-Dawley rat embryos. For pregnant rats from which embryos were harvested, the same euthanasia method as aforementioned was used. Only after confirmation of maternal death were the embryos collected under sterile conditions. Ganglia were cultured on six-well plates coated with poly-D-lysine (20 μg/ml) and laminin (overnight, 0.3 ml/well). The culture medium consisted of Neurobasal medium supplemented with B-27 (2%), L-glutamine (0.4 mM), glucose (2.5 mg/ml), fetal bovine serum (FBS; 1%, Gibco; Thermo Fisher Scientific, Inc.), and 2.5S nerve growth factor (10 ng/ml). Cytosine β-D-arabinofuranoside (5 μM), 5-fluoro-2'-deoxyuridine (20 μM), and uridine (20 μM) were added during the first 2 days to inhibit proliferation of non-neuronal cells (20).

To facilitate the transection of axons, a customized polydimethylsiloxane (PDMS) mold was designed. In brief, PDMS mixed with its curing agent (Sylgard 184; Corning, Inc.) in a ratio of 10:1 was poured into the wells of a six-well plate. After curing, a thick razor blade was used to carve two grooves intersecting with each other at the center of each PDMS mold. The long groove, 1.5 mm in width, was for accommodation of DRG, forcing the axons to grow bidirectionally, whereas the short groove, 2 mm in width, served as a slot for placement of a disposable razor blade that could gently transect the axons when they grew across the intersection. The DRG, cultured as aforementioned, were placed at ~1.5 mm away from the intersection, and the transfection was carried out at day 6. After transection, the DRG were assigned into the same four groups (no sham group) as in the mice experiment. The concentration was set at 10 μM for each inhibitor. On day 3, using the center of each DRG as the origin, the lengths of six regenerated axons, spaced at 30˚ intervals on the injured side, were measured as aforementioned and averaged to represent the lengths of regenerated axons of each DRG. Also, proteins were extracted from DRG in each group for western blotting, and Phalloidin and β-tubulin were used to respectively label the actin filaments and microtubules in the growth cones of DRG.

Immunofluorescence staining. SNs, spinal cords, and footpads were harvested at the designated time points, fixed in 4% paraformaldehyde (PFA) at room temperature overnight, dehydrated, and embedded in paraffin. Sections (7 μm) were deparaffinized and rehydrated. Antigen retrieval was performed in citrate buffer (pH 6.0) using a pressure cooker. After blocking with 5% normal goat serum for 1 h and permeabilization (0.3% Triton X-100), sections were incubated with primary antibodies overnight at 4˚C, followed by incubation with appropriate secondary antibodies for 1 h and DAPI (1 μg/ml) counterstaining. The same protocol was adapted for DRG samples after fixation in 4% PFA for 10 min, omitting the deparaffinization and antigen retrieval steps. The detail of the antibodies used are listed in Table I.

Table I. Information about antibodies used in the present study.

Antibody name	Manufacturer	Cat. no.	Dilution
Akt1 + Akt 2 + Akt3	Abcam	ab179463	1:1,000
GAP43	Proteintech Group, Inc.	16971-1-AP	1:1,000
Goat anti-Mouse IgG H&L 488	Beyotime Institute of Biotechnology	A0428	1:500
Goat anti-Rabbit IgG H&L CY3	Beyotime Institute of Biotechnology	A0516	1:500
Goat anti-Rabbit IgG H&L 647	Beyotime Institute of Biotechnology	A0468	1:500
GSK3β	Beyotime	AF5174	1:1,000
HRP-Goat Anti Mouse	Proteintech Group, Inc.	SA00001-1	1:500
HRP-Goat Anti Rabbit	Proteintech Group, Inc.	SA00001-2	1:500
Keratin 8	Wuhan Servicebio Technology Co., Ltd.	GB15231	1:2,000
Ki67	Wuhan Servicebio Technology Co., Ltd.	GB111141	1:500
MPZ	Beyotime Institute of Biotechnology	AF7497	1:200
NeuN	Proteintech Group, Inc.	26975-1-AP	1:2,000
Neurofilament 200	MilliporeSigma	N4142	1:200
Neurofilament 200	Wuhan Servicebio Technology Co., Ltd.	GB12143	1:5,000
Phospho-Akt (Ser473)	Cell Signaling Technology, Inc.	9271	1:1,000
Phospho-GSK3β (Ser9)	Cell Signaling Technology, Inc.	5558	1:1,000
Phospho-PI3K P85α/β/P55γ	Beyotime Institute of Biotechnology	AF5905	1:1,000
PI3K P85 beta	Beyotime Institute of Biotechnology	AF1729	1:1,000
Rho A	Wuhan Servicebio Technology Co., Ltd.	GB115177	1:1,000
Rhodamine phalloidin	Invitrogen; Thermo Fisher Scientific, Inc.	5210655	1:1,000
ROCK1/2	Abcam	ab45171	1:1,000
S100 beta	Wuhan Servicebio Technology Co., Ltd.	GB15359	1:2,000
a-bungarotoxin	Invitrogen; Thermo Fisher Scientific, Inc.	2286321	1:1,000
β-Tubulin (Tuj1)	Beyotime Institute of Biotechnology	AT809	1:1,000

Whole-mount staining of neuromuscular junction. On day 30 post-injury, the extensor hallucis longus muscle was dissected and fixed in 4% PFA for 1 h. Muscle bundles were teased apart (21) and permeabilized with 2% Triton X-100 overnight. Axons were stained with anti-NF-200 antibody, and acetylcholine receptors were labeled with Alexa 594-conjugated α-bungarotoxin (α-BGT). After imaging, the reinnervation rate of the endplate was calculated by dividing the immuno-positive area of NF-200 by the immuno-positive area of α-BGT in six random myofibers.

Western blotting. Lumbosacral enlargements (LEs; day 3 post-injury in mice) and pooled DRGs after *in vitro* axotomy (n=20/group) were homogenized in NP-40 lysis buffer (cat. no. ST2045; Beyotime Institute of Biotechnology) with protease and phosphatase inhibitors. Protein concentrations were determined using the BCA assay. Equal amounts (20 μg) of protein were separated by 10% SDS-PAGE and transferred to PVDF membranes. After blocking, membranes were probed with primary and HRP-conjugated secondary antibodies and visualized using enhanced chemiluminescence (IGEPAL® CA-630; cat. no. P0018S; Beyotime Institute of Biotechnology). Band intensity was quantified by ImageJ software (1.54p; National Institutes of Health) and normalized to loading controls. The detail of the antibodies used are listed in Table I.

Retrograde tracing with cholera toxin subunit B (CTB). A total of 3 weeks after SNC, 1 μl of Alexa Fluor 594-conjugated CTB (cat. no. C34777; Invitrogen; Thermo Fisher Scientific, Inc.) was injected 0.5 cm distal to the injury site in the right SN. A total of 7 days later, lumbosacral segments were collected, cryo-sectioned (30 μm), and CTB-labeled neurons were counted across all sections to quantify retrograde transport.

Functional assessment

Motor function. The Sciatic Function Index (SFI) was assessed at day 30 using footprint analysis. Key measurements included: heel-to-toe distance (print length, PL); distance between the first and fifth toes (toe spread, TS); and distance between the second and fourth toes (intermediary toe spread, IT). Data were collected for both the normal (N) and experimental (E) hindlimbs. The SFI was calculated using the formula: SFI= -38.3 x (EPL-NPL)/NPL + 109.5 x (ETS-NTS)/NTS + 13.3 x (EIT-NIT)/NIT-8.8.

Sensory function. Mechanical sensitivity was tested with Von Frey filaments; thermal sensitivity with a hot plate (55±1˚C). The paw withdrawal threshold and latency were recorded as average values over three trials.

Muscle strength and atrophy. At day 30, after anesthesia with sodium pentobarbital (50 mg/kg, i.p.), the gastrocnemius muscle was carefully separated from the surrounding musculature without damaging the blood supplies and nerves. A suture was tied around the calcaneal tendon, which was

detached from the calcaneus bone. The other end of the suture was then tied to a tension transducer, which was connected to a RM6240 Multi-Channel Physiological Signal Acquisition and Processing System (Chengdu Instrument Factory) for recording and analysis. The SN under the gluteus maximus was exposed and a stimulating electrode (Anhui Zhenghua Biological Instrument and Equipment Co., Ltd.) was placed upon it. The single-pulse stimulus mode with a pulse width of 0.2 ms was used. The voltage was started at 0.1 V and gradually increased in 0.05 V increments until reaching maximum isometric twitch force.

At day 30, the gastrocnemius muscle was dissected and weighed, and images for macroscopic analysis were captured. The ratio of the muscle weight on the experimental side to that on the normal side was calculated for each mouse. Muscles were then processed for paraffin embedding, and hematoxylin and eosin (H&E) staining was performed using a commercial kit (Solarbio, cat. no. G1120). The myofiber CSA was calculated from three randomly selected mid-belly fields (x20) and averaged using ImageJ (National Institutes of Health).

RSC96 cell proliferation and migration assays. For proliferation assay, $3x10^4$ Rat Schwann Cell Line (RSC96 cells) were cultured in Dulbecco's Modified Eagle Medium (DMEM; Thermo Fisher Scientific, Inc.) supplemented with 10% FBS (HyClone; Cytiva), and 1% penicillin/streptomycin (Beyotime Institute of Biotechnology). The cells were then divided into the control, Y27632, Y + LY, and Y + LY + SB groups, with DMSO and the relevant inhibitors added into the medium as aforementioned, together with 10 μM 5-ethynyl-2'-deoxyuridine (EdU) (Beyotime Institute of Biotechnology). A total of 24 h later, cells were fixed with 4% PDA for 15 min at room temperature, permeabilized with PBS containing 0.5% Triton X-100 for 20 min and then incubated with a reaction solution (cat. no. C0071S; Beyotime Institute of Biotechnology) for 30 min.

For the scratch assay, confluent monolayers were scraped with a pipette tip. Migration into the scratch area was monitored at 0 and 24 h using phase-contrast microscopy. Scratch closure rate was calculated as a percentage of baseline width.

Statistical analysis. Data are presented as the mean ± standard error of the mean (SEM). One-way ANOVA was used for group comparisons, with LSD or Dunnett's T3 post-hoc tests depending on variance homogeneity. Two-way ANOVA was used for DRG axon length analyses. $P<0.05$ was considered to indicate a statistically significant difference. The statistical analysis was performed with GraphPad Prism 8 (Dotmatics).

Results

Effects of three inhibitors on nerve regeneration after SNC. Following SNC, NF-200 immunostaining revealed a complete absence of axons at the clamp site (Fig. 1A and B), confirming successful model establishment. Compared with the experimental group, the Y27632 group showed a significantly increased density of regenerated axons at the clamp site on day 14 post-injury, calculated by normalizing the NF-200 immuno-positive area to 0.5 mm^2 (white box region) (Y27632 vs. experimental, P=0.0318). Notably, co-treatment with LY294002 significantly attenuated the pro-regenerative effect of Y27632 (Y + LY vs. Y27632, P=0.001). Strikingly, supplementation with SB216763 effectively reversed the adverse effects induced by PI3K inhibition (Y + LY + SB vs. Y + LY, P=0.0316; Fig. 1C and D).

Analysis of axonal CSA on day 30 revealed that Y27632 significantly increased axon diameter compared with the experimental group ($P<0.0001$), indicating accelerated maturation. By contrast, the axons in the Y + LY group reverted to baseline maturity levels (Y + LY vs. experimental, P=0.9001). This phenotype was completely reversed upon co-treatment of SB216763 (Y + LY + SB vs. Y + LY, $P<0.0001$; Fig. 1E and F).

Retrograde CTB tracing on day 30 demonstrated that both the Y27632 group and the Y + LY + SB group exhibited a remarkably significant increase in CTB-labeled neuron counts compared with the experimental group and the Y + LY group ($P<0.0001$; Fig. 1G-I).

ROCK inhibition promotes phosphorylation of PI3K/Akt/GSK3β in vivo. Western blot analysis showed that on day 3 after SNC in mice, the expression of RhoA and ROCK1/2 in the LE were significantly upregulated (Fig. 2A-C). Moreover, upregulation of regeneration-associated proteins GAP-43 and c-Jun confirmed ongoing repair processes (Fig. 2D and E). Treatment with Y27632 did not produce significant changes in RhoA or ROCK1/2 expression, but significantly enhanced the phosphorylation levels of PI3K, Akt and GSK3β compared with the experimental group (Fig. 2F-K). By contrast, co-treatment with LY294002 led to an ~50% reduction in GSK3β phosphorylation (Fig. 2L and M).

Immunofluorescence confirmed these findings: On day 3 after SNC, ROCK1/2 expression in the SN (calculated as the ratio of the ROCK1/2 immuno-positive area over the cross-section area of each nerve) and the LE (calculated from dividing the ROCK1/2-positive area by the NeuN-positive area) increased by 4.4-fold and 0.5-fold, respectively (SN: P=0.0002; LE: P=0.0333). Furthermore, Y27632 treatment could significantly elevate the expression of P-GSK3β in the SN and LE ($P<0.01$) (Fig. 2N-R).

ROCK inhibition promotes PI3K/Akt/GSK3β phosphorylation and axon regeneration in vitro. In the DRG axotomy model, robust regenerated axons could be observed extending across the transection mark by day 1 (Fig. 3A). Western blotting on day 3 after axotomy confirmed significant upregulation of RhoA, ROCK1/2, GAP43 and c-Jun (Fig. 3B-F), consistent with *in vivo* axotomy responses. Compared with non-axotomized controls, axon growth was significantly reduced after axotomy (Fig. 3Q).

Further analysis demonstrated that Y27632 treatment significantly elevated phosphorylation levels of PI3K, Akt and GSK3β (Fig. 3G-L), while LY294002 treatment reduced P-GSK3β levels by 3.9-fold (Fig. 3M and N). Morphometric analysis showed that Y27632 increased the length of regenerated axons from 1,139±33 to 1,966±56 μm, which was suppressed by LY294002 co-treatment (1,050±34 μm), but restored by further co-treatment with SB216763 (1,909±35 μm; $P<0.0001$; Fig. 3O and P).

ROCK/PI3K/Akt/GSK3β pathway regulates growth cone morphology. The morphology of the growth cones in the

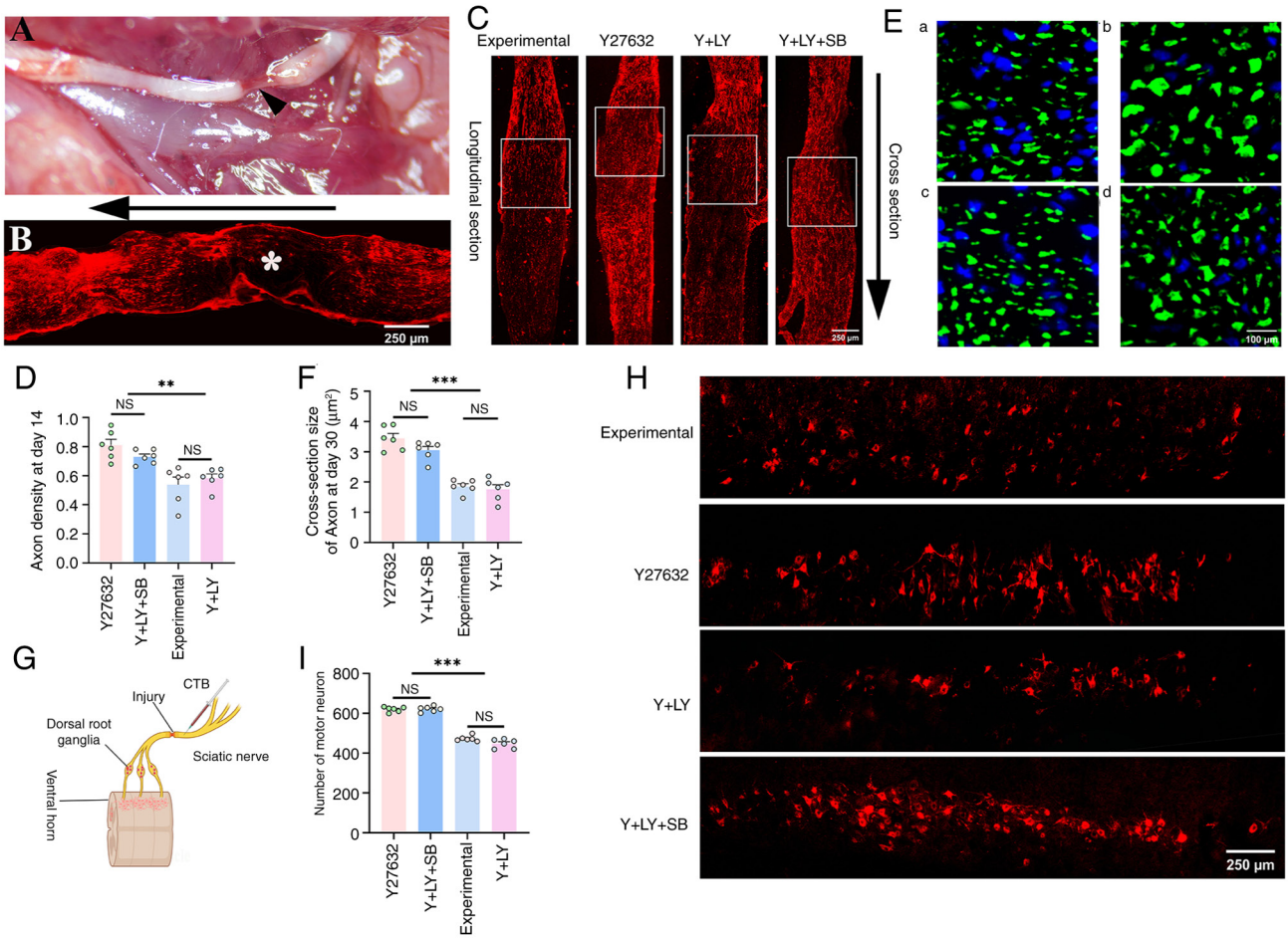

Figure 1. Effects of three inhibitors on nerve regeneration after SNC. (A) Representative gross image of a SN after SNC injury. The arrowhead indicates the formation of a nerve defect, with only the epineurium remaining after hemostat clamping. (B) The asterisk (*) marks a complete absence of NF-200-positive staining at the clamped site immediately after injury. The arrow denotes the proximal-to-distal orientation. (C) Representative longitudinal sections of injured nerves stained with NF-200 at day 14. (D) Axon density is significantly higher in the Y and Y + LY + SB groups (n=6). (E) Cross-sections stained with NF-200 on day 30 in all groups. a, b, c and d represent the staining from the experimental, Y27632, Y + LY, and Y + LY + SB groups, respectively. (F) The diameter of regenerated axons is significantly larger in the Y27632 and Y + LY + SB groups (n=6). (G) Schematic diagram of CTB injection into the SN distal to the clamped site for retrograde labeling of neurons in the ventral horn. (H and I) CTB-labeled neurons in the ventral horn are significantly more numerous in the Y27632 and Y + LY + SB groups (n=6). **P<0.01 and ***P<0.001. SN, sciatic nerve; SNC, SN crush; CTB, cholera toxin subunit B; NS, not significant (P>0.05).

experimental group was dramatically altered after axotomy. For the growth cones in the non-axotomy group, the phalloidin-positive actin in the periphery was broad, and the Tuj1-positive microtubule often splayed out at the end like a broom. Also, there was often a transition zone negative both in phalloidin and Tuj1. In comparison, after axotomy, the actin-rich area in the periphery was dramatically reduced, collapsing towards the microtubules, eliminating the transition zone, and the microtubules did not splay out at the end, resulting in a fivefold decrease in growth cone area (P<0.001). Y27632 treatment partially restored the growth cones morphology, including re-emergence of the transition zone and microtubule splaying. Statistically, Y27632 treatment enabled a 3-fold increase in the size of the growth cones, though still smaller than that in the non-axotomy group (Y27632 vs. Non-axotomy, P=0.002). This recovery was reversed by LY294002 and rescued by SB216763 (Fig. 4A-C).

ROCK/PI3K/Akt/GSK3β pathway regulates the recovery of motor and sensory functions. In terms of motor function, Y27632 increased gastrocnemius muscle recovery compared with the experimental and Y + LY groups (both P<0.001). SB216763 reversed the effect of LY294002 (Y + LY + SB vs. Y27632; P=0.2737) (Fig. 5A and B). Analysis of wet weight ratio showed that the Y27632 group had a 34.3% increase in gastrocnemius muscle weight compared with the experimental group (P=0.0045), while co-administration with LY294002 caused the weight to decrease by 28.9% (P=0.0015). Further co-administration with SB216763 reversed the inhibitory effect of LY294002, resulting in a 44.2% weight increase (P=0.0007). Cross-sectional H&E staining further confirmed this pattern. Further morphological investigation revealed that the reinnervation rate of the acetylcholine receptors in the Y27632 group was increased by 0.5-fold compared with the experimental group (P<0.0001), and there was no statistically significant difference between the Y27632 group and the Y + LY + SB group (P=0.3684) (Fig. 5C-F).

Gait analysis found that the SFI of the Y27632 group was significantly improved compared with that of the experimental group (P=0.0027) and the Y + LY group (P=0.0195) on day 14, and there was no significant difference compared with the Y + LY + SB group (P=0.6012), and this pattern persisted until day 30 after injury (Fig. 5G-J).

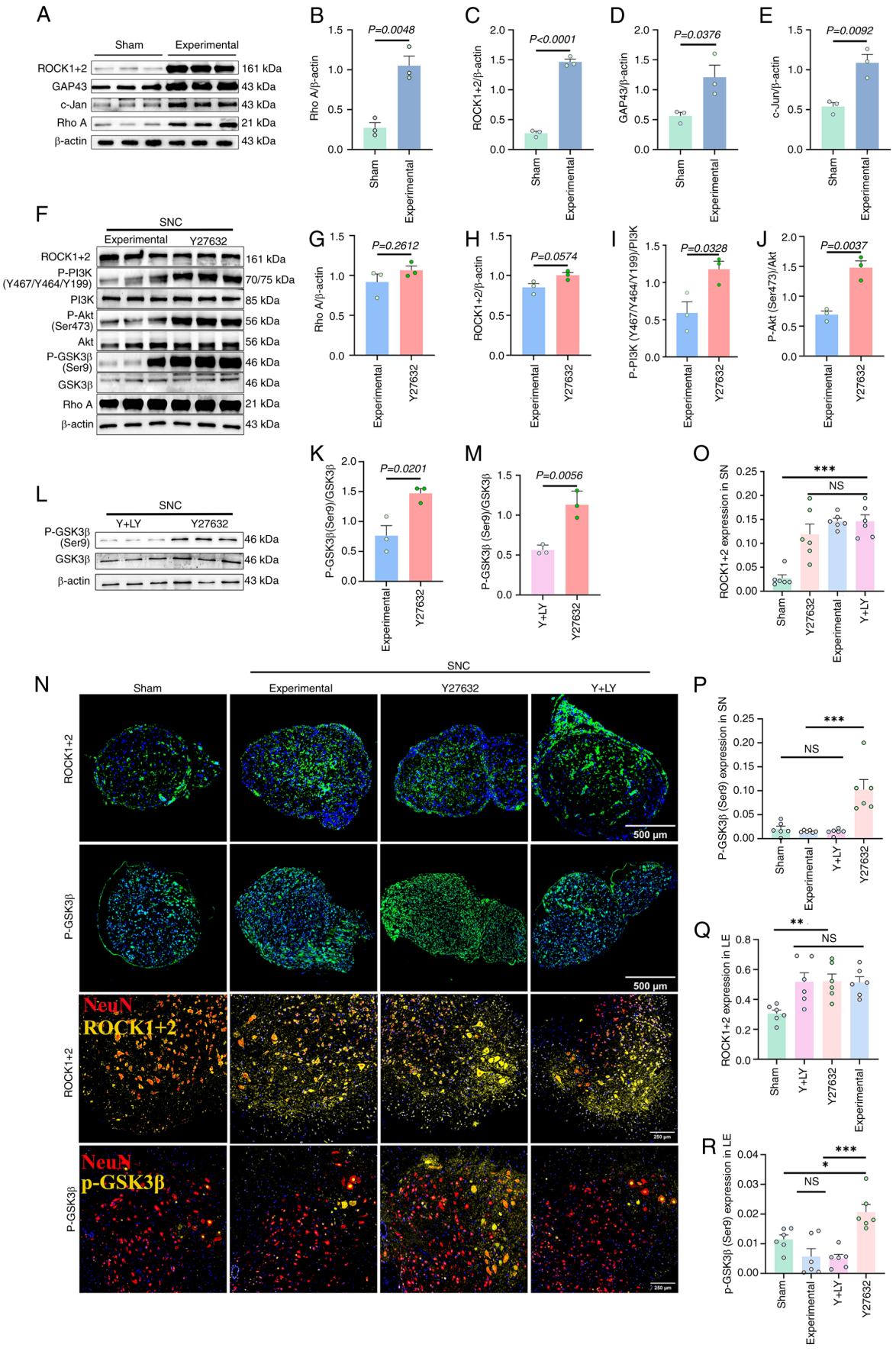

Figure 2. ROCK inhibition promotes phosphorylation of PI3K/Akt/GSK3β *in vivo*. (A-E) Increased expression of RhoA, ROCK1/2, GAP43 and c-Jun in the LE on day 3 after SNC (n=3). (F-K) Y27632 increases the phosphorylation of PI3K, Akt and GSK3β in the LE on day 3 after SNC (n=3). (L and M) Co-treatment with LY294002 reduces Y27632-induced phosphorylation of GSK3β (n=3). (N) Immunofluorescence images of ROCK1/2 and p-GSK3β in the sciatic nerve and LE. (O-R) Quantification of ROCK1/2 and P-GSK3β expression (n=6). *P<0.05, **P<0.01 and ***P<0.001. LE, lumbosacral enlargement; SNC, sciatic nerve crush; p-, phosphorylated; NS, not significant (P>0.05).

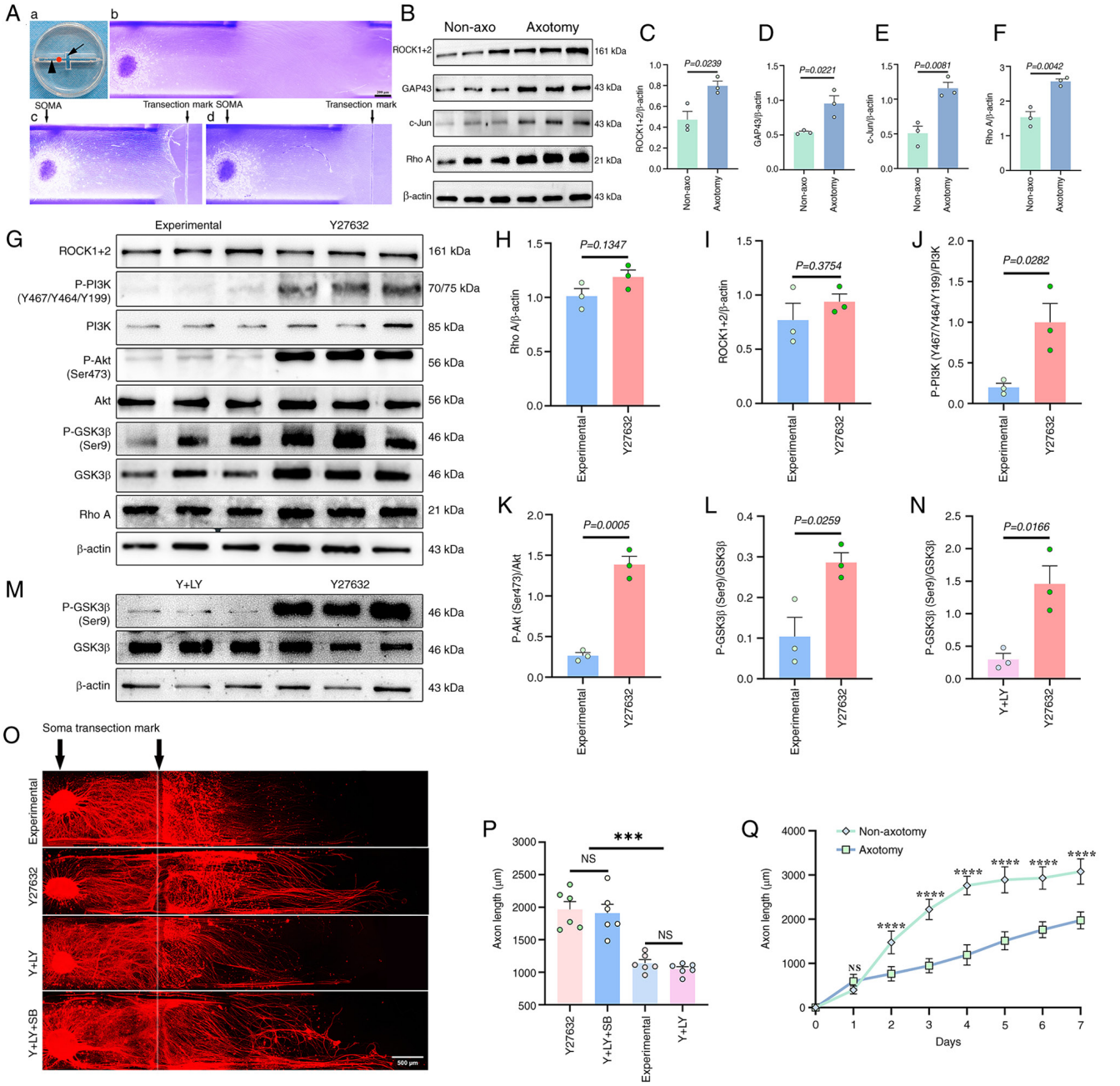

Figure 3. ROCK inhibition promotes PI3K/Akt/GSK3β phosphorylation and axon regeneration *in vitro*. (A-a), Customized polydimethylsiloxane mold: The arrowhead and arrow indicate the long and short grooves, respectively. The red spot indicates the site for placement of the DRG, ~1.5 mm away from the intersection. (A-b) Representative image of a DRG placed in the mold. (A-c) Representative image of the DRG immediately after axon transection. A shallow transection mark is left, and the distal stumps of the severed axons are washed away. (A-d) Regenerated axons emerging from the proximal stumps extend across the transection mark without obvious impediment. (B-F) The expression of RhoA, ROCK1/2, GAP43 and c-Jun is significantly elevated after axotomy (n=3). (G-L) Y27632 increases the phosphorylation of PI3K, Akt and GSK3β in the DRG on day 3 after axotomy (n=3). (M and N) LY294002 co-treatment reduces Y27632-induced phosphorylation of GSK3β (n=3). (O and P) The length of regenerated axons is significantly greater in the Y27632 and Y + LY + SB groups (n=5). (Q) Comparison of axon outgrowth in axotomized vs. non-axotomized DRG. ***P<0.001 and ****P<0.0001. DRG, dorsal root ganglion; NS, not significant (P>0.05).

In terms of sensory function, the morphological study demonstrated that Y27632 treatment increased the co-localization rate of Merkel cells and axons (calculated by the dividing the area of the axons labeled by NF-200 staining by that of the Merkel cells labeled by Keratin-8 staining) in the footpads by 5.8-fold (P<0.0001), and the treatment of SB216763 could reverse the inhibitory effect of LY294002 (P<0.0001), restoring the co-localization rate to 92.7% of the level of Y27632 treatment alone (P=0.1843, Fig. 5K and L). The morphological improvement in innervation in footpads translated to similar patterns of mechanical tactile and thermal pain sensation in the four groups (Fig. 5M and N).

ROCK/PI3K/Akt/GSK3β axis promotes remyelination and Schwann cell activity. Myelin sheath staining revealed that following Y27632 treatment, myelin sheath thickness in the injured area was 1.7- and 1.3-fold greater than that of the experimental and Y + LY groups, respectively (both P<0.001). The co-treatment with SB216763 also demonstrated a comparable remyelination-promoting effect, with the thickness

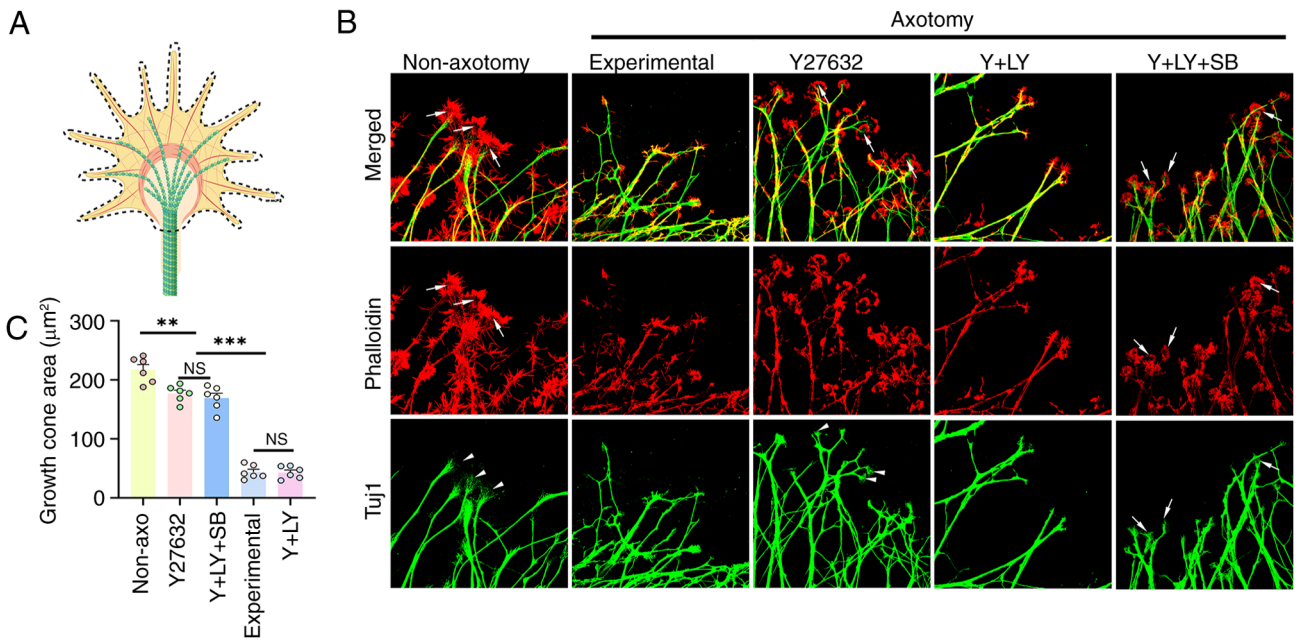

Figure 4. ROCK/PI3K/Akt/GSK3β pathway regulates growth cone morphology. (A) Schematic for growth cone size measurement. (B) Representative images of growth cones stained with Tuj1 and Phalloidin. Arrowheads indicate splayed microtubules; arrows mark transition zones. (C) Quantification of growth cone area (n=6). **P<0.01 and ***P<0.001. NS, not significant (P>0.05).

increasing by 1.1-fold relative to the Y + LY group (P<0.001; Fig. 6A and B). Furthermore, the proliferation rate of Schwann cells (calculated by dividing the number of S100β/Ki67 positive cells by the number of Ki67 positive cells in three random fields taken under x20 objective magnification) was significantly elevated by 1.1-fold on day 5 after SNC in the Y27632 group when compared with the experimental group (P<0.001). Similarly, this effect was abolished by LY294002 co-treatment and rescued by further SB216763 co-treatment (Fig. 6C and D).

In vitro, Y27632 enhanced EdU^{+} RSC96 cell proliferation by 1.3-fold (P=0.0003) and accelerated scratch closure rate by 0.8-fold (P<0.001). These effects were completely reversed by LY294002 and restored by SB216763, which even increased proliferation beyond Y27632 alone (P<0.005; Fig. 6E-H).

Discussion

The present study demonstrated that inhibition of ROCK via Y27632 significantly enhances axonal regeneration, remyelination, and functional recovery after axotomy. Mechanistically, these effects are mediated by activation of the PI3K/Akt signaling pathway and subsequent phosphorylation-mediated inhibition of GSK3β. These findings not only deepen our understanding of the molecular basis of peripheral nerve regeneration but also offer compelling evidence for the therapeutic potential of pharmacological modulation of the ROCK/PI3K/Akt/GSK3β signaling axis.

Western blot and immunofluorescence analyses in SNC model in mice demonstrated that Y27632 increased the phosphorylation levels of PI3K, Akt and GSK3β. Co-administration of the PI3K inhibitor LY294002 significantly suppressed GSK3β phosphorylation, validating the pathway's linearity and dependency. These molecular changes were associated with enhanced axonal regrowth and myelin sheath thickness, indicating that activation of this signaling axis not only initiates but sustains regenerative processes. However, this is one limitation that needs to be acknowledged here: the expression of proteins analyzed in mice was extracted from the LE, which sends motor axons into the SN. To strengthen the study, the expression of proteins in the $L_{4\text{-}6}$ DRG, which contribute sensory axons to the SN, should also be examined. However, challenges were faced in precisely identifying the $L_{4\text{-}6}$ DRG in mice. Additionally, the small size of murine DRGs presented significant obstacles for cryo-sectioning. This limitation needs to be addressed in future studies.

Histological and behavioral assessments further confirmed that Y27632 treatment translated to significant improvements in sensorimotor function. In terms of motor recovery, Y27632 enhanced neuromuscular junction reinnervation, reduced muscle atrophy, and increased gastrocnemius contractile strength. These results suggest that axons regenerated under ROCK inhibition are capable of functionally reconnecting with their target muscles. In terms of sensory function, Y27632 restores the integrity of Merkel complexes, which are formed by Merkel cells connecting with axons from slowly adapting type I Aβ low-threshold mechanoreceptor neurons, primarily responsible for tactile discrimination of object shape, curvature, and texture (22,23). The enhanced re-connection between Merkel cells and axons exemplifies improved growth of axons into the plantar skin, probably attributable to shortened thermal pain latency and reduced mechanical tactile threshold.

Importantly, the beneficial effects of Y27632 were largely abolished by PI3K inhibition and subsequently rescued by co-treatment with the GSK3β inhibitor SB216763. These findings identify GSK3β as a critical downstream effector mediating the pro-regenerative effects of ROCK inhibition. To the best of the authors' knowledge, this is the first study

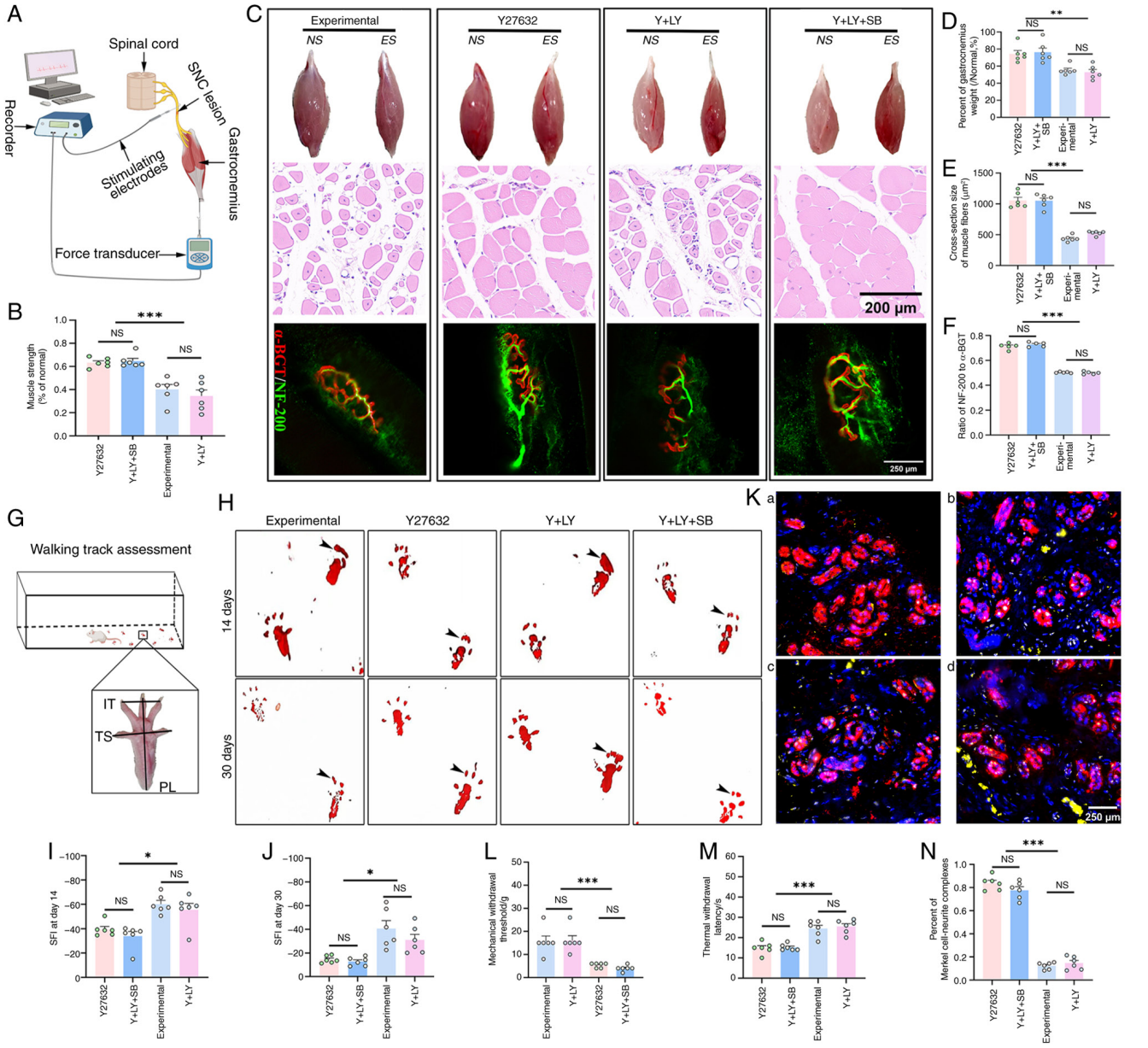

Figure 5. ROCK/PI3K/Akt/GSK3β pathway regulates locomotor and sensory recovery after sciatic nerve crush. (A) Experimental setup for muscle strength testing. (B) Gastrocnemius muscle strength ratio ES/NS was significantly greater in the Y27632 and Y + LY + SB groups (n=6). (C) Top row: Representative appearance of the gastrocnemius muscles on the NS and ES. Middle row: Representative cross-sections of the gastrocnemius muscles in ES. Bottom row: Representative neuromuscular junctions of the extensor hallucis longus on the ES. (D and E) The wet weight ratio and myofiber size were significantly larger in the Y27632 and Y + LY + SB groups (n=6). (F) The reinnervation rate of the acetylcholine receptor was significantly higher in the Y27632 and Y + LY + SB groups (n=6). (G) Schematic illustration evaluating the locomotor function using the sciatic function index. (H-J) Representative footprints demonstrated significantly improved recovery of locomotor function in the Y27632 and Y + LY + SB groups, as indicated by improved toe-spreading ability. (K) Representative images of reconnection between NF-200-labeled axons (Yellow) and Keratin 8-labeled Merkel cells (Red). Panels a, b, c and d represent typical images from the control, Y27632, Y + LY, and Y + LY + SB groups, respectively. (L) The reinnervation rate of the Merkel cells in the footpads was significantly higher in the Y27632 and Y + LY + SB groups (n=6). (M and N) Paw-licking latency and mechanical pain thresholds significantly improved in the Y27632 and Y + LY + SB groups (n=6). *P<0.05, **P<0.01 and ***P<0.001. ES, experimental side; NS, normal side; NS, not significant (P>0.05).

to delineate a functional ROCK → PI3K/Akt → GSK3β signaling cascade that governs axon regeneration and remyelination following PNI.

The regulation of the ROCK/PI3K/Akt/GSK3β pathway on axon regeneration can also be replicated in the *in vitro* DRG axotomy model, which is often adopted for the study of axon degeneration and regeneration (24,25). In this model, the upregulation of c-Jun and GAP-43, two common RAGs, along with upregulation of RhoA and ROCK mirrors the transcriptional programs that occur after nerve crush injury in mice (26-29), making it an ideal *in vitro* model for the investigation of molecular pathways relating to axon regeneration. In this context, Y27632 significantly promoted axonal elongation and growth cone expansion in a PI3K/GSK3β-dependent manner. One noteworthy point is that in this *in vitro* axotomy model, the original anatomical location of the DRG, whether from cervical, thoracic, or lumbar, is irrelevant, as each extracted DRG underwent axotomy, and treated with various agents as described. Another noteworthy point is that the *in vivo* experiments were performed in adult

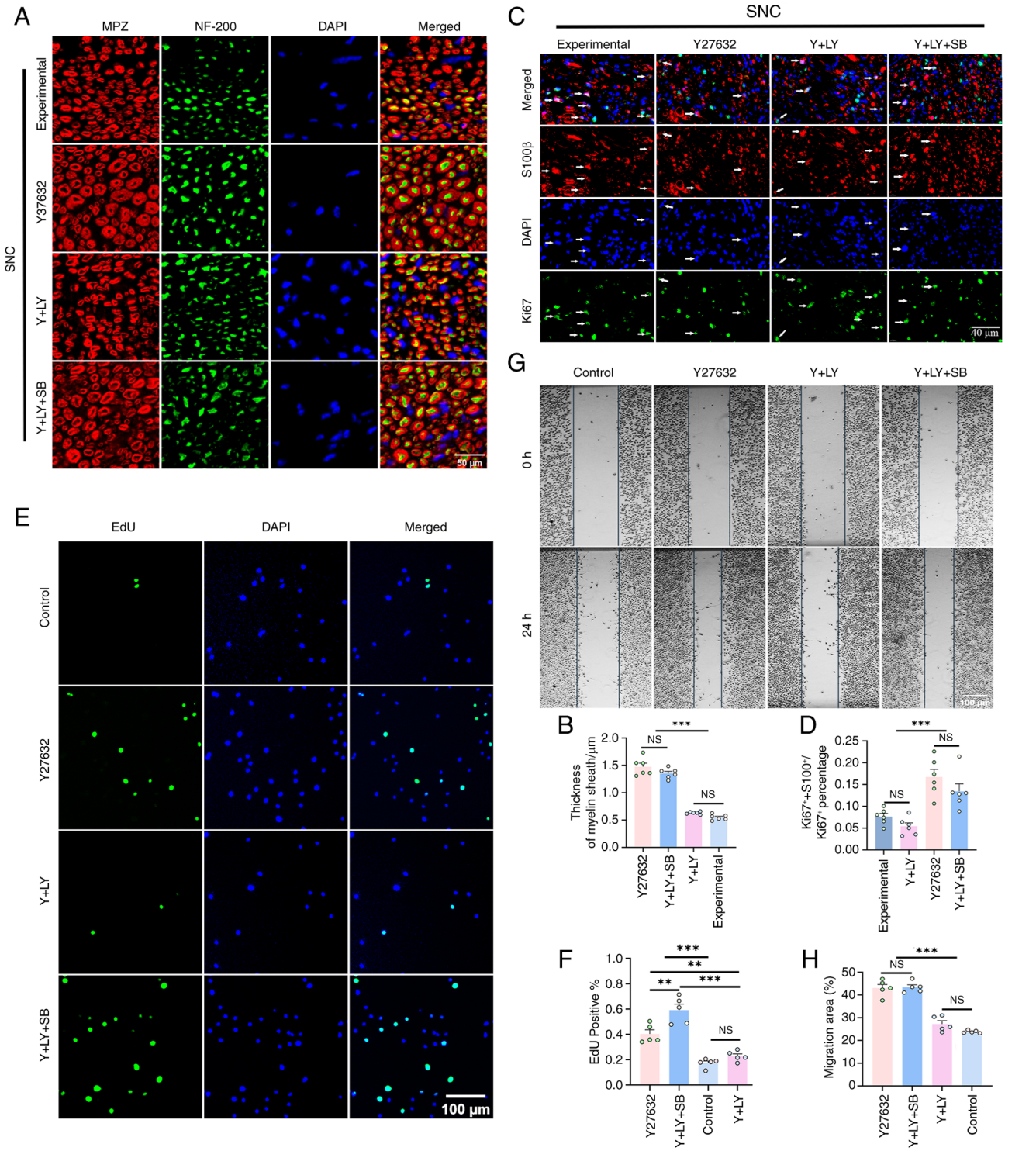

Figure 6. ROCK/PI3K/Akt/GSK3β Pathway regulates remyelination after SNC. (A) Representative images of axon and myelin staining at day 30. (B) The thickness of myelin sheaths was significantly greater in the Y27632 and Y + LY + SB groups (n=6). (C) Schwann cell proliferation assessed by S100β and Ki67 co-labeling on day 3 after SNC. (D) The proliferation rate of Schwann cells was significantly higher in the Y27632 and Y + LY + SB groups (n=6). (E and F) EdU assay showing increased RSC96 cell proliferation in the Y27632 and Y + LY + SB groups. (G and H) Scratch assay showing increased migration of RSC96 cells in the Y27632 and Y + LY + SB groups. NS, P>0.05; **P<0.01 and ***P<0.001. SNC, sciatic nerve crush; NS, not significant (P>0.05).

mice while the *in vitro* DRG axotomy model used embryonic rat ganglia. Although these differ in species and developmental stage, the core signaling modules investigated, RhoA/ROCK, PI3K/Akt and GSK3β, are evolutionarily conserved across vertebrates and across developmental contexts (10,30,31).

The growth cone, a specialized structure at the tip of extending axons, plays a pivotal role in sensing guidance cues and mediating cytoskeletal rearrangements (32,33). It is composed of actin at the periphery and microtubules at the core. As demonstrated in the present study, the size of growth cones after axotomy is drastically reduced after injury, shrinking the

thickness of the actin-rich periphery, eliminating the transition zone and broom-like end of the microtubule, probably due to the upregulation of the RhoA/ROCK pathway. The transition zone is abundant in myosin, which interacts with the actin to generate the force required to advance the growth cone along the substrate (34). Additionally, it has been reported that splaying out of microtubule into the periphery allows for interplay between the actin and microtubule and is conducive to axon growth. Therefore, the disappearance of the transition zone and microtubule splaying out is likely responsible for the significant slowing down of axon outgrowth after axotomy.

As expected, Y27632 can significantly expand the size of the growth cones, restoring the transition zone, and partially restores the broom-like appearance of the microtubule ends. The size of the growth cones then shrinks after co-treatment with LY294002 and expands again after further co-treatment with SB216763, suggesting the involvement of the ROCK/PI3K/Akt/GSK3β pathway in regulating the morphogenesis of the growth cones. Since it has been shown that Y27632 treatment can significantly increase the phosphorylation of GSK3β in DRG, and it is well established that increased phosphorylation of GSK3β can dephosphorylate MAPs, such as CRMP-2, MAP1B and APC, increasing their microtubule-binding affinity and thereby stabilizing microtubules to promote axon growth, it can be hypothesized that Y27632 may promote axon regeneration through stabilizing microtubules mediated by PI3K/Akt/GSK3β. While ROCK inhibition is well known to decrease MLC phosphorylation and reduce actomyosin contractility, how the PI3K/Akt/GSK3β axis intersects with actomyosin dynamics remains unclear and warrants future investigation.

The current data also suggest that ROCK inhibition promotes Schwann cell proliferation, migration, and myelin sheath formation, all of which are essential for peripheral nerve regeneration. These effects were also dependent on the PI3K/Akt/GSK3β pathway. Notably, previous *in vitro* studies have reported conflicting results regarding the role of ROCK inhibition in Schwann cell-mediated myelination, with some describing aberrant or discontinuous myelin formation (35). By contrast, the current *in vivo* data consistently show enhanced remyelination and functional recovery. These discrepancies may reflect context-dependent differences between *in vitro* co-culture systems and the more complex *in vivo* microenvironment.

A key limitation of the present study is the reliance on systemic administration of pharmacological inhibitors, which may have off-target effects. Although dosages were carefully matched across groups, these compounds are not neuron-specific and may influence other signaling cascades in peripheral or central tissues. Future studies should employ cell type-specific conditional knockout models to further dissect the roles of ROCK, PI3K and GSK3β in distinct neural populations, such as neurons versus Schwann cells.

In conclusion, the novelty of the present study lies in identification of GSK3β as a critical downstream effector of ROCK inhibition in the context of peripheral nerve regeneration. Although previous studies have shown that ROCK inhibition can activate PI3K/Akt signaling (11,12), the present study is, to the best of the authors' knowledge, the first to demonstrate that PI3K/Akt-mediated phosphorylation and inactivation of GSK3β are required for the regenerative effects on both axon and myelin sheath of ROCK inhibition. This elucidation of the downstream pathway lays an important foundation for exploring pharmaceutical agents targeting different nodes in this pathway individually or combinatorially for improving therapeutic effects of PNI.

Acknowledgements

The authors gratefully thank Ms Ling Lin and Mr Xi Lin from the public technology service center (Fujian medical university, Fuzhou, China) for technical assistance.

Funding

The present study was supported by Fujian provincial fund for joint scientific innovation (grant nos. 2024Y9096 and 2024Y9644) and Fujian Natural Science Fund (grant nos. 2025J01689 and 2025J01091).

Availability of data and materials

The data generated in the present study may be requested from the corresponding author.

Authors' contributions

SD and ZL were involved in the conceptualization of the study, performed the experiments, analyzed the data, and drafted the initial manuscript. FF contributed to the experimental design and retrograde tracing experiments. BZ performed *in vitro* experiments. ZR and HW provided expertise in clinical relevance and functional recovery assessments. QZ contributed to the histological and immunofluorescence analyses. YZ conceptualized the study, supervised the study, acquired funding, provided critical resources, interpretated the data, reviewed and edited the manuscript. All authors read and approved the final version of the manuscript. SD and YZ confirm the authenticity of all the raw data.

Ethics approval and consent to participate

All animal procedures were approved (approval no. 2024-Y-0566) by the Institutional Animal Care and Use Committee of Fujian Medical University (Fuzhou, China) and complied with the National Institutes of Health guidelines and ARRIVE standards.

Patient consent for publication

Not applicable.

Competing interests

The authors declare that they have no competing interests.

Use of artificial intelligence tools

During the preparation of this work, artificial intelligence tools were used to improve the readability and language of

the manuscript or to generate images, and subsequently, the authors revised and edited the content produced by the artificial intelligence tools as necessary, taking full responsibility for the ultimate content of the present manuscript.

References

1. Lavorato A, Aruta G, De Marco R, Zeppa P, Titolo P, Colonna MR, Galeano M, Costa AL, Vincitorio F, Garbossa D and Battiston B: Traumatic peripheral nerve injuries: A classification proposal. J Orthop Traumatol 24: 20, 2023.
2. Chiono V and Tonda-Turo C: Trends in the design of nerve guidance channels in peripheral nerve tissue engineering. Prog Neurobiol 131: 87-104, 2015.
3. Yadav A and Dabur R: Skeletal muscle atrophy after sciatic nerve damage: Mechanistic insights. Eur J Pharmacol 970: 176506, 2024.
4. Miclescu A, Straatmann A, Gkatziani P, Butler S, Karlsten R and Gordh T: Chronic neuropathic pain after traumatic peripheral nerve injuries in the upper extremity: Prevalence, demographic and surgical determinants, impact on health and on pain medication. Scand J Pain 20: 95-108, 2019.
5. Sulaiman W and Gordon T: Neurobiology of peripheral nerve injury, regeneration, and functional recovery: from bench top research to bedside application. Ochsner J 13: 100-108, 2013.
6. Wariyar SS and Ward PJ: Application of electrical stimulation to enhance axon regeneration following peripheral nerve injury. Bio Protoc 13: e4833, 2023.
7. Guo S, Moore RM, Charlesworth MC, Johnson KL, Spinner RJ, Windebank AJ and Wang H: The proteome of distal nerves: Implication in delayed repair and poor functional recovery. Neural Regen Res 17: 1998-2006, 2022.
8. Liu J, Wada Y, Katsura M, Tozawa H, Erwin N, Kapron CM, Bao G and Liu J: Rho-associated coiled-coil kinase (ROCK) in molecular regulation of angiogenesis. Theranostics 8: 6053-6069, 2018.
9. Guan G, Cannon RD, Coates DE and Mei L: Effect of the Rho-Kinase/ROCK signaling pathway on cytoskeleton components. Genes (Basel) 14: 272, 2023.
10. Fujita Y and Yamashita T: Axon growth inhibition by RhoA/ROCK in the central nervous system. Front Neurosci 8: 338, 2014.
11. Wang H, Fang F, Chen S, Jing X, Zhuang Y and Xie Y: Dual efficacy of Fasudil at improvement of survival and reinnervation of flap through RhoA / ROCK / PI3K /Akt pathway. Int Wound J 19: 2000-2011, 2022.
12. Wang H, Fang F, Jing X, Xu D, Ren Z, Dou S, Xie Y and Zhuang Y: Augmentation of functional recovery via *ROCK/PI3K/AKT* pathway by Fasudil Hydrochloride in a rat sciatic nerve transection model. J Orthop Transl 47: 74-86, 2024.
13. Zhang J, Yang S-G and Zhou F-Q: Glycogen synthase kinase 3 signaling in neural regeneration in vivo. J Mol Cell Biol 15: mjad075, 2024.
14. Ma Q, Chen G, Li Y, Guo Z and Zhang X: The molecular genetics of PI3K/PTEN/AKT/mTOR pathway in the malformations of cortical development. Genes Dis 11: 101021, 2024.
15. Li D, Qu Y, Mao M, Zhang X, Li J, Ferriero D and Mu D: Involvement of the PTEN-AKT-FOXO3a pathway in neuronal apoptosis in developing rat brain after hypoxia-ischemia. J Cereb Blood Flow Metab 29: 1903-1913, 2009.
16. Kitagishi Y, Nakanishi A, Ogura Y and Matsuda S: Dietary regulation of PI3K/AKT/GSK-3β pathway in Alzheimer's disease. Alzheimers Res Ther 6: 35, 2014.
17. Barnat M, Benassy M-N, Vincensini L, Soares S, Fassier C, Propst F, Andrieux A, von Boxberg Y and Nothias F: The GSK3-MAP1B pathway controls neurite branching and microtubule dynamics. Mol Cell Neurosci 72: 9-21, 2016.
18. Leibinger M, Hilla AM, Andreadaki A and Fischer D: GSK3-CRMP2 signaling mediates axonal regeneration induced by *Pten* knockout. Commun Biol 2: 318, 2019.
19. Juanes MA, Isnardon D, Badache A, Brasselet S, Mavrakis M and Goode BL: The role of APC-mediated actin assembly in microtubule capture and focal adhesion turnover. J Cell Biol 218: 3415-3435, 2019.
20. Shekarabi M, Robinson JA and Burdo TH: Isolation and culture of dorsal root ganglia (DRG) from rodents. Methods Mol Biol 2311: 177-184, 2021.
21. Schüler SC, Dumontier S, Rigaux J and Bentzinger CF: Visualization of the skeletal muscle stem cell niche in fiber bundles. Curr Protoc 1: e263, 2021.
22. Bataille A, Le Gall C, Misery L and Talagas M: Merkel cells are multimodal sensory cells: A review of study methods. Cells 11: 3827, 2022.
23. Fleming MS and Luo W: The anatomy, function, and development of mammalian Aβ low-threshold mechanoreceptors. Front Biol (Beijing) 8: 408-420, 2013.
24. Assessing axonal degeneration in embryonic dorsal root ganglion neurons in vitro. In: Methods in Molecular Biology. Springer US, New York, NY, pp41-54, 2020.
25. George E, Glass J and Griffin J: Axotomy-induced axonal degeneration is mediated by calcium influx through ion-specific channels. J Neurosci 15: 6445-6452, 1995.
26. Joshi AR, Bobylev I, Zhang G, Sheikh KA and Lehmann HC: Inhibition of Rho-kinase differentially affects axon regeneration of peripheral motor and sensory nerves. Exp Neurol 263: 28-38, 2015.
27. Liu K, Tedeschi A, Park KK and He Z: Neuronal intrinsic mechanisms of axon regeneration. Annu Rev Neurosci 34: 131-152, 2011.
28. Hiraga A, Kuwabara S, Doya H, Kanai K, Fujitani M, Taniguchi J, Arai K, Mori M, Hattori T and Yamashita T: Rho-kinase inhibition enhances axonal regeneration after peripheral nerve injury. J Peripher Nerv Syst 11: 217-224, 2006.
29. Saijilafu, Hur E-M, Liu C-M, Jiao Z, Xu W-L and Zhou F-Q: PI3K-GSK3 signalling regulates mammalian axon regeneration by inducing the expression of Smad1. Nat Commun 4: 2690, 2013.
30. Hemmings BA and Restuccia DF: PI3K-PKB/Akt Pathway. Cold Spring Harb Perspect Biol 4: a011189, 2012.
31. Zhang X, Zhao G, Yang F, Li C, Lin W, Dai H, Zhai L, Xi X, Yuan Q and Huo J: Transcriptional regulation analysis provides insight into the function of *GSK3β* gene in Diannan small-ear pig spermatogenesis. Genes (Basel) 15: 655, 2024.
32. Alfadil E, Bradke F and Dupraz S: In situ visualization of axon growth and growth cone dynamics in acute ex vivo embryonic brain slice cultures. J Vis Exp 176: 1-24, 2021.
33. Nakajima C, Sawada M, Umeda E, Takagi Y, Nakashima N, Kuboyama K, Kaneko N, Yamamoto S, Nakamura H, Shimada N, *et al*: Identification of the growth cone as a probe and driver of neuronal migration in the injured brain. Nat Commun 15: 1877, 2024.
34. Santos TE, Schaffran B, Broguière N, Meyn L, Zenobi-Wong M and Bradke F: Axon growth of CNS neurons in three dimensions is amoeboid and independent of adhesions. Cell Rep 32: 107907, 2020.
35. Melendez-Vasquez CV, Einheber S and Salzer JL: Rho kinase regulates schwann cell myelination and formation of associated axonal domains. J Neurosci 24: 3953-3963, 2004.